# Commissioning a Testing Chamber for DAMIC CCD Development

Benjamin Siegel[1]
Advisor: Alvaro E. Chavarria[2]
*1-University of California Santa Barbara*
*2-University of Washington*

(2018 INT REU, University of Washington)
(Dated: Aug. 30, 2018)

The goal of the DAMIC project is to detect dark matter particles via scattering in charged-coupled devices (CCDs). This report presents the current progress on commissioning a surface level test chamber at the University of Washington. This test chamber will be used to develop the next generation of CCD to be used in dark matter detection. To handle CCDs for performance testing, the chamber must be able to maintain a vacuum under $10^{-4}$ mBar, cool CCDs to temperatures of 100-150 Kelvin, and cool at a rate less than 5 Kelvin per minute.

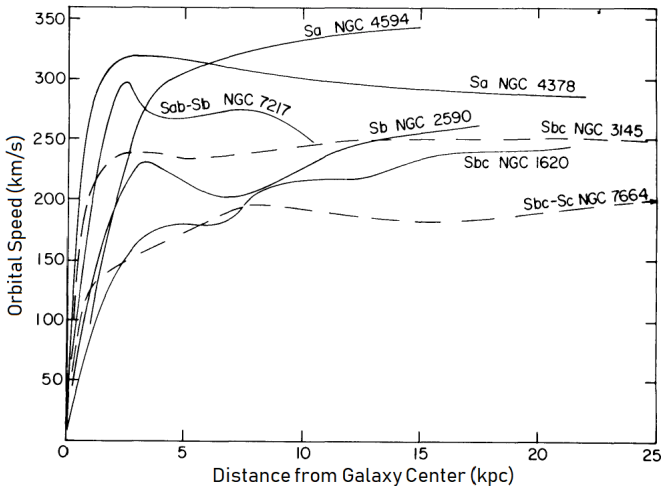


FIG. 1. Orbital Speed as a function of distance to galaxy center for seven galaxies. The orbital speeds do not fall off with increased radius as Keplerian calculations predict [9].

## I. INTRODUCTION

Dark matter was proposed partially as a solution to gravitational inconsistencies. One such problem is the high orbital speed of stars in the outer reaches of many galaxies. Rubin, Ford and Thonnard in 1978 showed that the relation between orbital speed of stars and their distance from the center of their galaxy is relatively flat with the outer edges displaying a rotational velocity of 20 km $s^{-1}$ higher than inner edges [9], as shown in Fig. 1. Keplerian predictions would model a decreasing orbital speed with increasing radius based on the distribution of luminous and visible matter in galaxies. This implies that there is an additional massive halos extending to large radii which signifies galaxy mass to increase significantly with radius and rotational velocities to remain high [9]. Dark matter is a possible gravitational source in such halos.

Current models of dark matter, such as axions and weakly interaction massive particles (WIMPs), propose a dark matter particle. In the axion model particles have small masses in the range of $\mu$eV to mev. Axions are pseudo-scalar bosons proposed to explain the smallness of observations, such as the magnetic moment of neutrons, of strong charge conjugation parity violations[7]. Although they have a light mass, axions weak coupling leave them as a possible candidate due to not attaining thermal equilibrium with the early universe. WIMPs are a cold dark matter candidate, which means they are non-relativistic and bound to the galaxies. Most dark matter studies focus on searching for WIMPs with masses in the range of GeV - TeV. In the supersymmetry model, WIMPs are a likely candidate for massive neutral particles due to spontaneous symmetry breaking[7]. WIMPs are a promising possible dark matter particle due to the "Weak Miracle". This implies "if one assumes approximately weak-scale cross sections for the cold dark matter annihilation process, one obtains a dark matter relic density consistent with cosmological measurements"[7]. Possible methods to detect WIMPs include searching for evidence of annihilation events, creating WIMPs in accelerators or looking for scattering of WIMPs with baryonic matter[7]. The last of these is the approach under consideration here.

### A. Dark Matter in CCDs Experiment (DAMIC)

The DAMIC (Dark Matter in CCDs) experiment's aim is to detect coherent elastic scattering of dark matter particles via the silicon bulk in charged-coupled detectors[2] as displayed in Fig. 2. The target energy levels in consideration correspond mostly to the weakly interaction massive particle model of dark matter[2]. The sensitivity of the CCDs, limited by the relatively low mass of silicon nuclei, is ideal for low mass WIMPs, $1-10$ Gev $c^{-2}$, which would correspond to keV-scale nuclear recoils[4]. A detailed review of such recoil events is given by Lewin and Smith[6]. To minimize other events producing signals, DAMIC is conducted two kilometers underground

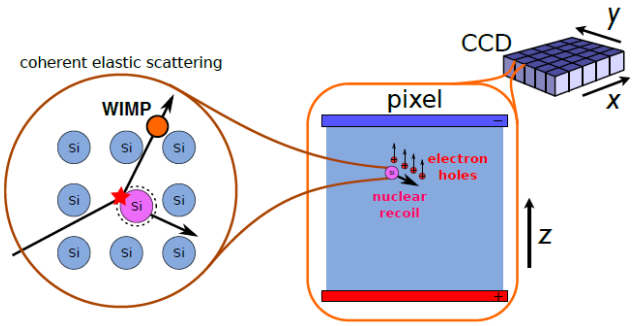


FIG. 2. Diagram of a WIMP elastically scattering off a silicon nucleus in the bulk of a CCD. This scattered nucleus transfers some of its kinetic energy to ionization in the CCD. Due to a bias voltage placed on the top and bottom of the CCD, these ionized electron holes drift in the positive z direction of the figure [1].

with polyethylene and lead shielding, shown in Fig. 3, to block cosmic muons, environmental neutrons and $\gamma$-rays respectively[1]. The innermost lead layer is sourced from an ancient Spanish galleon for its negligible amount of $^{210}$Pb. This layer strongly suppresses the $^{210}$Bi $\gamma$-decays from the outer lead layers. The current DAMIC project uses seven CCDs inside a copper box. This box, is cooled to $\sim$ 120 K inside a copper vacuum chamber at $\sim 10^{-6}$ mBar[1, 2]. Cooling is required to reduce dark current. Dark current is leakage current from the pixels caused by thermal excitations. At 120 K, dark current magnitudes of $10^{-3}e^-$ pixel$^{-1}$ day$^{-1}$ have been observed [2, 5].

### B. CCD Operation

The ionized charge created from recoil events is transported out of the CCD using voltage phase cycles. A CCD is divided into pixels by $SiO_2$ etchings on the surface. Each pixel is subdivided into three regions with electrodes, as in Fig. 4. The ionized holes drift towards these electrodes, held in the silicon bulk by a p-channel. The holes are moved along the pixels via a three phase voltage cycle in the electrodes. The first electrode is set to a negative voltage while the other two are high. Then, the neighboring electrode is set to a negative voltage while the first one is set high. This new electric field attracts the holes to the second electrode. The process is repeated with the second and third electrodes[8]. As shown in Fig. 5, the three different electrodes along all the pixels are connected so that when the holes are held by the third electrode of one pixel, they can be moved along to the next pixel by setting $\Phi^1$ negative and $\Phi^3$ high[8]. Repeating this voltage cycle moves the holes to the edges of the CCD, where another phase cycle moves them to a readout node. This phase cycle on the edges runs faster to ensure that the charge collected from each pixel is kept independent of other pixel's charges. Once the charge has been measured, the value can be ascribed to a certain pixels location in the CCD based on the time it reached the readout node[8].

The readout node measures the charge using correlated double sampling. The voltage of the readout node is integrated over for a long period of time while it is empty. This is called the noise pedestal. Then a pixel's charge is transfered to the readout node and the voltage is measured in the same way. Integration over a 40 $\mu$s total time period suppresses high frequency noise[2]. Using the difference between the pedestal noise measurement and the charge measurement leads to suppression of correlated electronic noise in the readout chain[2].

## II. COMMISSIONING THE CHAMBER

The surface level testing chamber being commissioned at the University of Washington will be used to characterize the performance of CCDs packaged at the University of Washington and for developing the next generation of CCDs. To do this, it must be capable of cooling to 100-150 K at sub $10^{-4}$ mBar pressures[3]. The low pressure ensures no condensation or particulate interaction occurs on the CCD surface, while this temperature range is used to limit the dark current, as previously mentioned. Additionally, to limit the thermal stress on the CCD, the test chamber must be able to heat and cool at sub 5 Kelvin per minute rates[3].

The test chamber, depicted in Fig. 6, is composed of a Cryotel GT cryocooler and controller, a Pfeiffer vacuum pump and gauge system, a Lake Shore Model 325 Temperature Controller, a 25 $\Omega$ resistor heating element, a liquid cooling system for the cryocooler and a Leach readout system. The CCD is held in an aluminum box. This is attached to a copper bar that is attached via a brass screw to the cold tip of the cryocooler. The resistor heating element and cryocooler controller's temperature sensor are attached to the copper bar close to the cold tip.

To test CCDs, first, the chamber is pumped down to, at maximum, $2 * 10^{-4}$ mBar. Once it has reached the desired pressure, the CCD is cooled down. In cooling, the resistor heating element is necessary to provide enough of a thermal load for the cryocooler to stay stable at the target temperature. Once it is cooled sufficiently to suppress dark current, images can be taken with the CCD using the Leach readout system.

### A. Temperature Control

Initially, the Lake Shore heater was not used, and the temperature control system consisted only of the Cryotel cryocooler. Initial testing indicated that a heater was necessary to provide enough of a thermal load for the cryocooler to operate properly. When not enough of a thermal load is applied, the cryocooler will cool beyond the input desired temperature. This is due to the

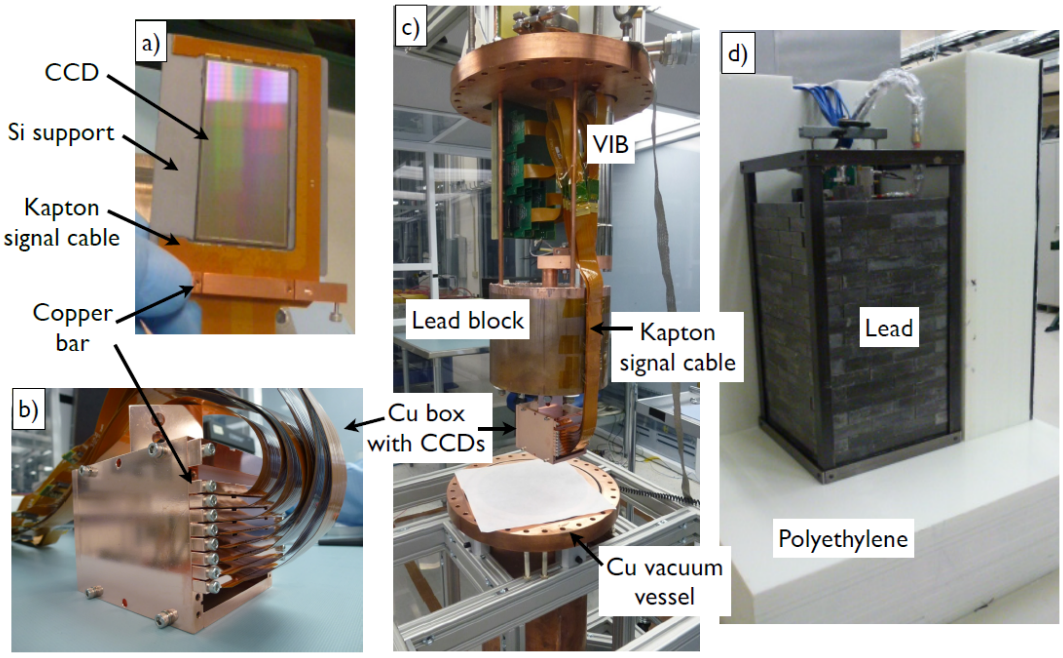


FIG. 3. Experimental setup of DAMIC at SNOLAB. The experiment is conducted about 2 km underground to prevent eliminate cosmic muons. There are shielding layers of polyethylene and lead to suppress environmental neutrons and $\gamma$ rays respectively. Inside these shielding layers is a copper vacuum vessel. Inside the vessel, the CCD are held in copper boxes and surrounded by a layer of ancient lead. This ancient lead suppresses $\gamma$-rays, especially from decay of the outer shielding layer of lead.[1].

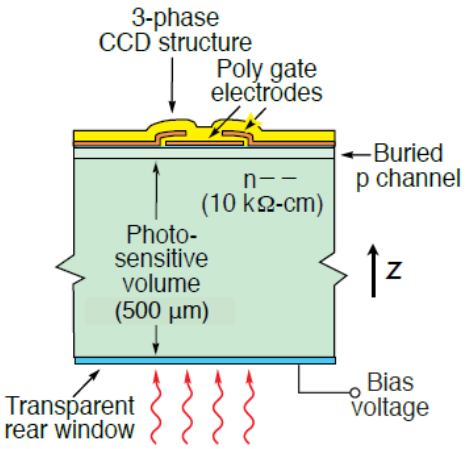


FIG. 4. Diagram of a CCD pixel cross section. The bulk silicon is where charge is ionized from events. This charge drifts in the positive z direction due to the bias voltage placed on the rear of the CCD. On the front of the CCD pixel are three electrodes which move the charge across the front of the CCD. These electrodes are behind a buried p-channel of silicon to ensure charge does not escape the pixel [1].

cryocooler power range. When reaching the desired temperature, the cryocooler attempts to find a power level that maintains a stable temperature. If this happens to be below the minimum power level, which is 70 W for most temperatures, then it will use the minimum power level. This causes continued cooling until balance has been reached with the thermal load and the cryocooler. An example of too low of a thermal load is using 5 W heater power. This results in cooling past the desired temperature and becoming stable at $\sim$ 115 K. By including the Lake Shore heater, the thermal load can be increased to an appropriate value so that the cryocooler finds a power level within its operating range to keep the temperature stable. The heater cannot be set arbitrarily high for a similar reason. If the thermal load is too great, the rate of heating will balance with the rate of cooling of the cryocooler at its maximum power. In this case, the temperature control system reaches a stable point above the desired temperature and will not cool further. For instance, setting the heater power to 15 W corresponds to preventing cooling past $\sim$ 180 K, and setting the heater power to 12.5 W corresponds to preventing cooling past $\sim$ 145 K. Table I shows the recommended heater powers for optimal operation of the temperature control system.

In addition to choosing a heater power to ensure the CCD cools down to the desired temperature, the heater power and cryocooler power must be varied based on the current temperature to prevent cooling too quickly. Without this dynamic control of power settings, the temperature control system cools quicker than 5 K per minute from when it is started at room temperature until it has reached $\sim$ 250 K. An example of this is Fig. 7, which depicts the temperature rate of change when

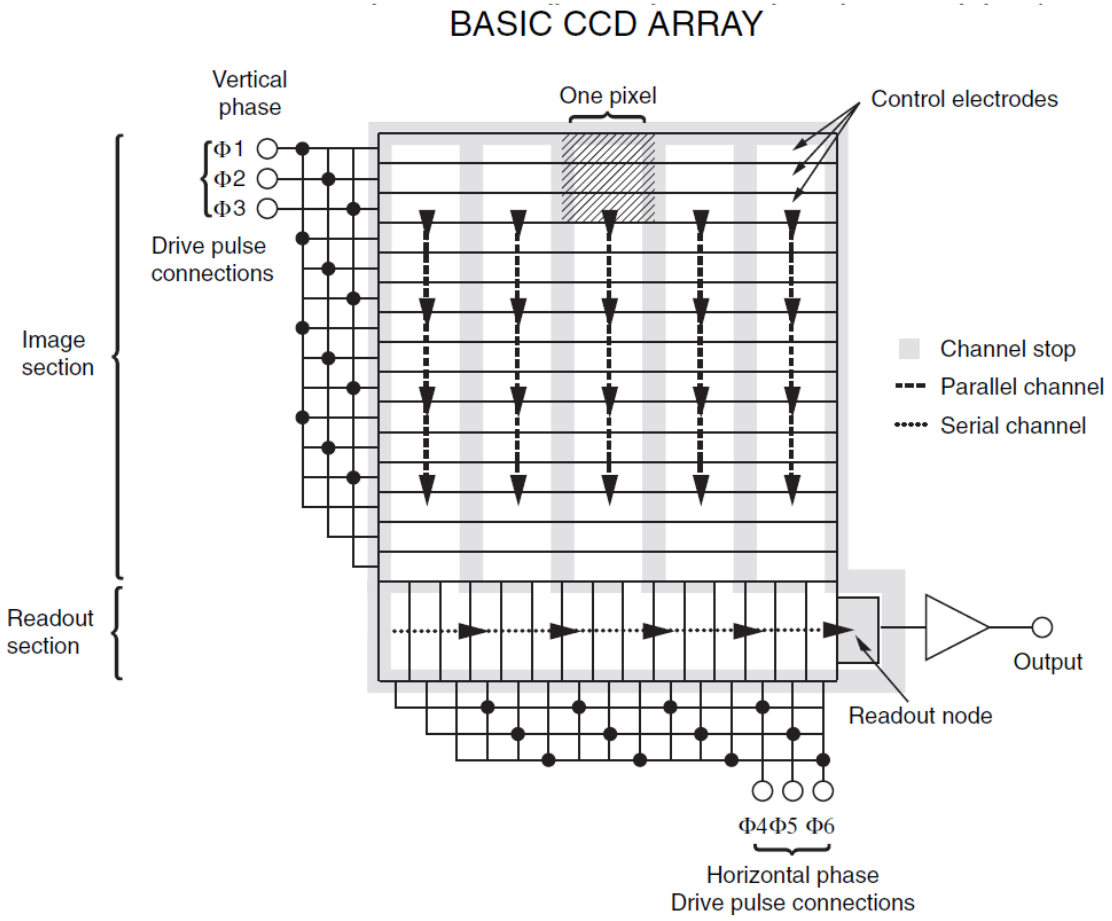


FIG. 5. Schematic of the phases used to transport charge across the CCD. As one control electrode turns on, the previous one turns off to move charge down the CCD. All of the pixels' electrodes are synced for transfer of charge from one pixel to the next. Vertical $SiO_2$ etchings prevent charge from moving to a different column of pixels. When the charge reaches the edge, other electrodes move charge along the edge to the readout node in a similar manner [8].

| Heater Power (W) | Desired Temperature (K) |
|---|---|
| 12.5 | 150-170 |
| 10 | 140-150 |
| 7.5 | 125-140 |
| 6.25 | 115-125 |
| 5 | 100 - 115 |

TABLE I. The heater power settings in watts that corresponds to successfully cooling to temperatures within the corresponding ranges.

cooling to 150 K using a constant heater power of 12.5 W. To prevent this, an automated script was created for the cool down process. This script changes the heater power setting and sets the maximum power limit for the cryocooler based on the current temperature. The script is set to cool at a maximum rate of 4 Kelvin per minute. The success of automating the cooling process is shown by Fig. 7.

## III. TAKING IMAGES WITH A CCD

Once the temperature control system was setup, images were taken with the Leach readout system. Initial images show that the CCD was clocking properly and the readout system functioned. Fig. 8 is a 1000x800 pixel section of an image taking in the newly commissioned chamber. Due to not being isolated like at the DAMIC setup at SNOLAB tracks can be seen from $\alpha$ particles, excited electrons, and muons ionizing charge on the CCD, as depicted in Fig. 8. Electrons tracks present as curling lines, muon interactions present as straight tracks where the length of the track depends on the muon's angle of incidence with the CCD. $\alpha$ particles display as circular tracks[1]. Even though there is no phase clocking in the depth dimension of the CCD, the depth of events (z-position as shown in Fig. 4) can be determined by the spread of charge[2]. The lateral dispersion of charge is positively correlated with depth of the event from the electrodes. The CCD currently used for testing displays

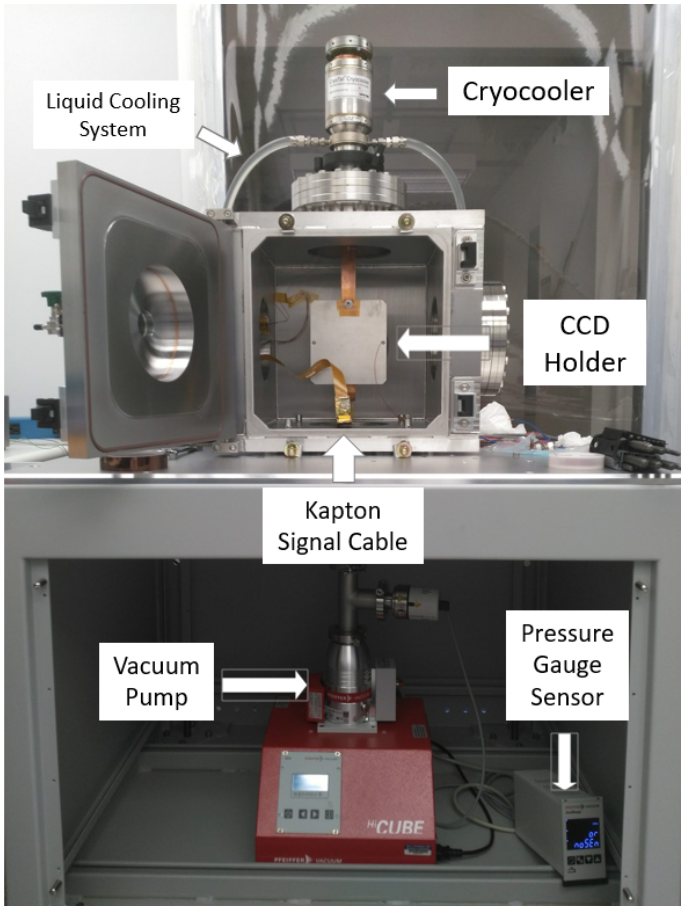


FIG. 6. The surface level testing chamber being commissioned at the University of Washington. Here the CCD is held withing a aluminum box supported by a copper bar. This copper bar attaches to a cryocooler. The CCD is inside a steel vacuum chamber which is capable of reaching pressures sub-$10^{-4}$ mBar. A liquid cooling system is attached to the cryocooler housing to prevent overheating.

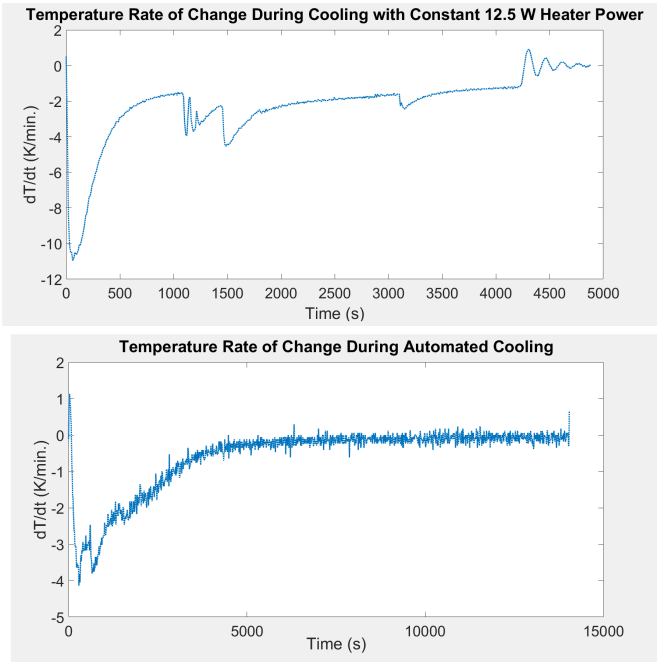


FIG. 7. Plots of the temperature's rate of change during cooling down the CCD. The top plot's data was taken with a constant heater power of 12.5 W. The bottom plot's data is taken with a variable heater power that is a function of the current temperature. In order to limit thermal stress on the CCD, the rate of change is desired to be below 5 K per minute, which the variable heater power test achieves.

some defects among the columns of pixels, represented by a straight vertical line that is constant across multiple images. When processing many images, such defects can be removed by creating a mask. The mask ignores pixels which display high energy readings in all of the images being processed.

## IV. NOISE

The desired noise level is 2 eV, which is the base noise level from the amplifiers in the readout system[1]. The first images indicated a much higher noise level, with large contributions originating from outside the readout system.

The cryocooler sourced a large amount of problematic noise as shown by Fig. 9, which compares an image taken with the cryocooler on and no preventative measures taken to one taken with the cryocooler off. With the cryocooler on, correlated noise is visible as a pattern, whereas with the cryocooler off, it appears to be white noise. Further probing with an oscilloscope revealed that the cryocooler generated $28 \pm 2$ kHz square waves. Noise on this timescale is especially problematic due to the similar integration time as discussed above. This noise on the same timescale as the integration period leads to a modified difference between the pedestal noise measurement or the charge measurement. Based on whether the charge measurement was increased or decreased relative to the pedestal measurement by the noise, the measurement of each pixel can be artificially higher or lower. The offset in the integration period and noise period causes a cycle of artificially high and low measurements, which appears as the pattern shown in Fig. 9.

Other contributions to the noise include wave packet bursts. 1 $\mu$s wide bursts were injected into the signal by the cryocooler's switching power supply likely due to the switching of its transistor. This noise was present when the switching power supply was plugged in, even if the cryocooler was not running.

Additionally, sinusoidal noise was observed. High frequency 1 MHz waves were seen in the CCD output signal while the CCD temperature was above 200 K. This noise disappeared though when cooled down to the operating range. Low frequency waves of $700 \pm 50$ Hz and $156 \pm 10$ Hz were present as well. The $700 \pm 50$ Hz noise

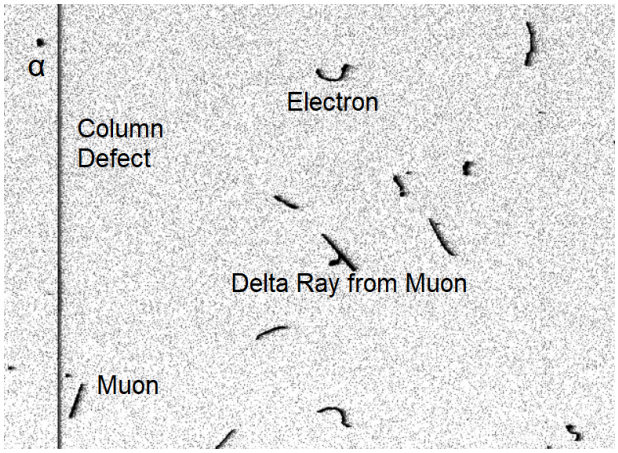


FIG. 8. 1000 pixel by 800 pixel image taken in the surface level test chamber at the University of Washington. The different shaped tracks correspond to different events as labeled in the image. Circular tracks are $\alpha$ particles. Straight tracks are muons traveling through the CCD. Curling tracks are excited electrons moving in the CCD. The long vertical line is a defect among that column of pixels causing them all to saturate [4].

is possibly caused by the vacuum pump, as its operating speed is 1500 Hz. The $156 \pm 10$ Hz noise was from a ground loop created by the test chamber being grounded via a copper braid and through the readout system. This noise is partially mitigated by correlated double sampling measurements. Integrating leads to decreased contribution of high frequency (relative to the integration time) noise, and low frequency noise is essentially flat for one double correlated sampling measurement. The electrical connection between the chamber and the readout system affected the overall noise level as well. When increasing the amount of contact between the readout system and chamber, the noise of the CCD output signal, observed on an oscilloscope, decreases significantly.

### A. Mitigation Attempts

To reduce the noise to a usable level many different approaches have been tried. For the $28 \pm 2$ kHz noise, electrical and vibrational isolation was tested. The cryocooler cold tip was covered in Kapton tape to electrically isolate the cryocooler from the CCD aluminum holder. To reduce vibrations from the cryocooler piston affecting the CCD holder, it was suspended with a copper braid. Both had no noticeable effect on the noise, as it was discovered that it was RF noise likely caused by a switching component in the cryocooler controller. This noise was eliminated by electrically connecting the CCD holder and the test chamber using a thin Kapton wire. This wire is thought to act as a path of less resistance for the noise to reach ground rather than going through the Kapton signal cable to the readout system.

In response to the $1\mu s$ wave packets, the readout system and cryocooler power supply were plugged into different outlets to decrease their interaction through ground. This was effective, as the noise amplitude decreased by about a factor of two. Further grounding separation and addition of ferrite cores to the wires leading to the cryocooler controller reduced the noise amplitude even further. To completely remove this noise, the switching power supply was replaced with a linear power supply. Since linear power supplies use transformers alone, there is no element switching on and off to create noise bursts. Unfortunately, the Acopian 48V DC linear power supply has a maximum output current of 8.5A, while the cryocooler can draw up to 10A in the process of cooling down. The lack of current causes the cryocooler to malfunction, as has been observed when cooling at 120 K with a heater power of 5W. When cooled down and maintaining a stable temperature, only $5 \pm 1$A are drawn, so the linear power supply can still be used while at temperature and taking images.

## V. CALIBRATION OF ENERGY LEVELS

A radioactive source's $\gamma$ emission was used to determine the current noise energy levels and convert the readout system's Analog-Digital Units (ADU) to electron volts. Initial energy calibration used Americium-241 sources placed on the outside of the steel testing chamber. The Americium-241's 59.5 keV $\gamma$ rays produced events with values of $143.5 * 10^3$ ADU. Since the electron-hole creation energy for silicon is 3.7 eV, the conversion rate between ADU and electrons is 9 ADU per electron. With the observed noise of $36 \pm 4$ ADU for one of the CCD readout channels and $40 \pm 4$ ADU for the second channel using the noise mitigations steps described above, there is a noise of $5 \pm 1$ electrons. This is 3 electrons greater than the desired noise level.

## VI. CONCLUSION AND FUTURE WORK

In summary, a surface test chamber has been commissioned at the University of Washington. This test chamber is capable of holding sub-$10^{-4}$ mBar pressures. It can cool CCDs to a temperature within 100-150 K at rates of less than 5 K per minute. Most of the initial noise issues have been solved, yet there is still readout noise of over 2 electrons greater than desired. Future work on the test chamber will reduce the noise level to the base amplifier noise level. A more intensive solution to the cryocooler square wave noise might be pursued by constructing a controller that does not exhibit this noise or attaching a filter to block the controller's noise from reaching the test chamber. Once an acceptable noise level has been reached, this test chamber will be used in the development of the next generation of CCDs and in checking the performance of CCDs packaged at the University of Washington.

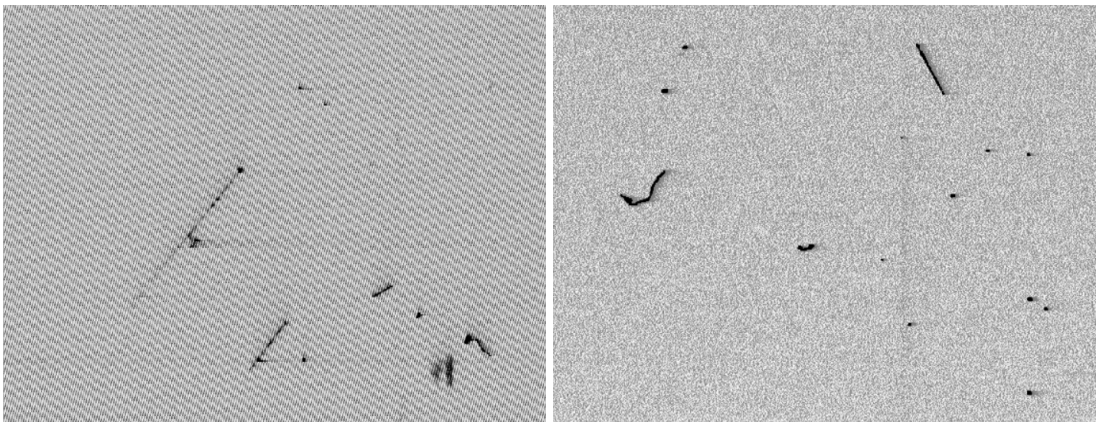

FIG. 9. Two images taken that display the effects of the $28 \pm 2$ kHz square wave noise from the cryocooler. The image on the left was taken with the cryocooler on and no preventative measures taken to reduce the noise. The image on the right was taken with the cryocooler off. With the cryocooler on, there is a definite pattern in the noise due to the noise being around the same order of magnitude as the charge measuring integration period.

## VII. ACKNOWLEDGEMENTS

This work was supported through the National Science Foundation through the University of Washington Physics Research Opportunity for Undergraduates. I thank Dr. Grey Rybka and Dr. Subhadeep Gupta for coordinating this REU as well as the the administrative staff Linda Vilett and Cheryl McDaniel. I am grateful for Dr. Alvaro Chavarria's guidance on this project and thank Dr. Pitam Mitra and graduate student Alex Piers for their help.

[1] A. Aguilar-Arevalo, D. Amidei, X. Bertou, D. Bole, M. Butner, G. Cancelo, A. Castañeda Vásquez, A. E. Chavarria, J. R.T. De Mello Neto, S. Dixon, J. C. D'Olivo, J. Estrada, G. Fernandez Moroni, K. P. Hernández Torres, F. Izraelevitch, A. Kavner, B. Kilminster, I. Lawson, J. Liao, M. López, J. Molina, G. Moreno-Granados, J. Pena, P. Privitera, Y. Sarkis, V. Scarpine, T. Schwarz, M. Sofo Haro, J. Tiffenberg, D. Torres Machado, F. Trillaud, X. Yol, and J. Zhou. Measurement of radioactive contamination in the CCD's of the DAMIC experiment. *Journal of Physics: Conference Series*, 718(4), 2016. ISSN 17426596. doi:10.1088/1742-6596/718/4/042057.

[2] A. Aguilar-Arevalo, D. Amidei, X. Bertou, M. Butner, G. Cancelo, A. Castañeda Vázquez, B. A. Cervantes Vergara, A. E. Chavarria, C. R. Chavez, J. R.T. De Mello Neto, J. C. D'Olivo, J. Estrada, G. Fernandez Moroni, R. Gaïor, Y. Guardincerri, K. P. Hernández Torres, F. Izraelevitch, A. Kavner, B. Kilminster, I. Lawson, A. Letessier-Selvon, J. Liao, V. B.B. Mello, J. Molina, J. R. Peña, P. Privitera, K. Ramanathan, Y. Sarkis, T. Schwarz, C. Sengul, M. Settimo, M. Sofo Haro, R. Thomas, J. Tiffenberg, E. Tiouchichine, D. Torres Machado, F. Trillaud, X. You, and J. Zhou. Search for low-mass WIMPs in a 0.6 kg day exposure of the DAMIC experiment at SNOLAB SEARCH for LOW-MASS WIMPs in A 0.6 KG DAY ... A. AGUILAR-AREVALO et al. *Physical Review D*, 94(8):1–11, 2016. ISSN 24700029. doi: 10.1103/PhysRevD.94.082006.

[3] C Bebek and N Roe. 4k x 2k and 4k x 4k CCD Users Manual Table of Contents. 2011.

[4] A E Chavarria. DAMIC at SNOLAB.

[5] Rouven Essig, Marivi Fernández-Serra, Jeremy Mardon, Adrián Soto, Tomer Volansky, and Tien Tien Yu. Direct detection of sub-GeV dark matter with semiconductor targets. *Journal of High Energy Physics*, 2016(5), 2016. ISSN 10298479. doi:10.1007/JHEP05(2016)046.

[6] J. D. Lewin and P. F. Smith. Review of mathematics, numerical factors, and corrections for dark matter experiments based on elastic nuclear recoil. *Astroparticle Physics*, 6(1):87–112, 1996. ISSN 09276505. doi: 10.1016/S0927-6505(96)00047-3.

[7] BM Loer. Towards a depleted argon time projection chamber WIMP search: Darkside prototype analysis and predicted sensitivity. (November), 2011. URL `http://adsabs.harvard.edu/abs/2011PhDT.....137L`.

[8] J B Pawley. More Than You Ever Really Wanted to Know AboutCharge-Coupled Devices. *Handbook of Biological Confocal Microscopy*, pages 918–931, 2006.

[9] V. C. Rubin, N. Thonnard, and Jr. Ford, W. K. Extended rotation curves of high-luminosity spiral galaxies. IV - Systematic dynamical properties, SA through SC. *The Astrophysical Journal*, 225(3):L107, 1978. ISSN 0004-637X. doi:10.1086/182804. URL `http://adsabs.harvard.edu/doi/10.1086/182804`.